Monthly Notices of the ROYAL ASTRONOMICAL SOCIETY

MNRAS **460,** 3940–3949 (2016) doi:10.1093/mnras/stw1254
Advance Access publication 2016 May 26

Planetary nebulae in the Small Magellanic Cloud

P. Ventura,[1]★ L. Stanghellini,[2] M. Di Criscienzo,[1] D. A. García-Hernández[3,4] and F. Dell'Agli[1]

[1]*INAF–Osservatorio Astronomico di Roma, Via Frascati 33, I-00040 Monte Porzio Catone (RM), Italy*
[2]*National Optical Astronomy Observatory, 950 N. Cherry Avenue, Tucson, AZ 85719, USA*
[3]*Instituto de Astrofísica de Canarias, E-38205 La Laguna, Tenerife, Spain*
[4]*Departamento de Astrofísica, Universidad de La Laguna (ULL), E-38206 La Laguna, Tenerife, Spain*

Accepted 2016 May 23. Received 2016 May 23; in original form 2016 February 26

ABSTRACT

We analyse the planetary nebulae (PNe) population of the Small Magellanic Cloud (SMC), based on evolutionary models of stars with metallicities in the range $10^{-3} \leq Z \leq 4 \times 10^{-3}$ and mass $0.9\,M_{\odot} < M < 8\,M_{\odot}$, evolved through the asymptotic giant branch (AGB) phase. The models used account for dust formation in the circumstellar envelope. To characterize the PNe sample of the SMC, we compare the observed abundances of the various species with the final chemical composition of the AGB models: this study allows us to identify the progenitors of the PNe observed, in terms of mass and chemical composition. According to our interpretation, most of the PNe descend from low-mass ($M < 2\,M_{\odot}$) stars, which become carbon rich, after experiencing repeated third dredge-up episodes, during the AGB phase. A fraction of the PNe showing the signature of advanced CNO processing are interpreted as the progeny of massive AGB stars, with mass above $\sim 6\,M_{\odot}$, undergoing strong hot bottom burning. The differences with the chemical composition of the PNe population of the Large Magellanic Cloud is explained on the basis of the diverse star formation history and age–metallicity relation of the two galaxies. The implications of this study for some still highly debated points regarding the AGB evolution are also commented.

Key words: Stars: abundances – Stars: AGB and post-AGB – Stars: carbon.

1 INTRODUCTION

The final phases in the evolution of stars of intermediate mass ($0.8\,M_{\odot} \leq M \leq 8\,M_{\odot}$) is still poorly known, owing to the uncertainties affecting the understanding of the asymptotic giant branch (AGB) phase. The two main factors preventing reliable AGB modelling are the treatment of the convective instability, and that of the mass-loss mechanism, which are still rather uncertain (Herwig 2005; Karakas & Lattanzio 2014). As a consequence, the role played by AGB stars in several astrophysical contexts is still highly debated. On the other hand, understanding the AGB impact is crucial for several astrophysical fields, such as the determination of the masses of galaxies at high redshifts (Maraston et al. 2006), the formation and chemical evolution of galaxies (Romano et al. 2010; Santini et al. 2014), the dust content of high-redshift quasars (Valiante et al. 2011), and the formation of multiple populations of stars in globular clusters (Ventura et al. 2001).

Following the pioneering studies by the Heidelberg group (Ferrarotti & Gail 2006), some authors have recently made significant progresses in AGB modelling when including the formation of dust in the circumstellar envelopes of AGB stars (Ventura et al. 2012a,b, 2014b; Di Criscienzo et al. 2013; Nanni et al. 2013a,b, 2014).

Testing these models requires comparison with the observations. The Magellanic Clouds (MC) have so far offered the best comparison laboratory, owing to their relatively short distances [51 and 61 kpc, respectively, for the Large Magellanic Cloud (LMC) and Small Magellanic Cloud (SMC), Cioni et al. 2000; Keller & Wood 2006 and the low reddening [$E(B-V) = 0.15$ and 0.04 mag, respectively, for the LMC and SMC, Westerlund 1997]. Furthermore, the study of the MC populations extends to a wide range of metallicities, broadening the possible comparison between data and models, and are less affected by interstellar extinction than Galactic populations.

The near- and mid-infrared observations of AGB stars in the MC, compared with the evolutionary models produced by various research teams, allowed the empirical calibration of the physical mechanisms relevant to the evolution of these objects. For example, such comparisons have allowed primarily to estimate

★ E-mail: paolo.ventura@oa-roma.inaf.it

the extension of the third dredge-up (hereinafter TDU), i.e. the inwards penetration of the bottom of the convective envelope in the phase following each thermal pulse (Izzard et al. 2004; Girardi & Marigo 2007; Groenewegen et al. 2007; Srinivasan et al. 2009; Riebel et al. 2010, 2012; Boyer et al. 2011, 2012; Srinivasan, Sargent & Meixner 2011). More recent studies were focused on the dust production by AGB stars in the MC and the characterization of the most obscured sources (Dell'Agli et al. 2014, 2015a,b; Ventura et al. 2015a, 2016).

The study of planetary nebulae (PNe) offers an alternative opportunity to constrain the evolutionary models that evolve through the AGB. In fact, the surface chemistry of AGB stars will eventually contribute to the chemical mix of the ejected PNe. By studying the PN abundances we can infer the combined effects of the physical mechanisms potentially able to alter the surface chemical composition of AGB stars. In particular, two main processes are active in this chemical transformation of the stellar surface, namely, the TDU, and the hot bottom burning (HBB), i.e. the proton capture nucleosynthesis active at the base of the envelope of the stars whose initial mass is above $\sim 4\,M_{\odot}$ (Renzini & Voli 1981; Blöcker & Schöenberner 1991). Knowledge of the nebular chemical composition of PNe allows us to understand the relative importance of these phenomena on the modification of the surface chemical composition during the whole AGB evolution (Marigo et al. 2003, 2011). Another advantage of using PNe to constrain AGB evolutionary models resides in the fact that PN abundance analysis is relatively straightforward in comparison to that of AGB stars, whose optical- and near-IR spectra are contaminated by millions of molecular lines, which render extremely complex the derivation of the abundances of individual species (e.g. García-Hernández et al. 2006, 2007, 2009).

Since the evolutionary properties of AGB stars might depend on the environment where they have formed and evolved (e.g. the initial medium composition, the density of stars, etc.), it is mandatory to study the nebular abundances in different PN populations (e.g. at several metallicities) and compare them with models of different initial mass and chemistry. The MC PN populations seem to be ideally suited for these comparisons.

Here, we focus on the comparison between AGB stellar evolution and nucleosynthesis models and PNe observed in the SMC. Our goals are both the identification of particular PN populations to be associated with specific AGB processes, and the refinement in our understanding of the main physical aspects of AGB evolution. This analysis is complementary to the interpretation of observed samples of AGB stars, which is based on the straight comparison between the evolutionary sequences through the AGB and the sources observed.

In the first paper of this series (Ventura et al. 2015, hereafter Paper I), we interpreted the PNe observed in the LMC in terms of mass, formation epoch, and chemical composition of their progenitors, based on the comparison of observational data with the evolutionary AGB models. Paper I confirmed that the models used to reproduce the *Spitzer* observations of evolved stars in the LMC (Dell'Agli et al. 2015a) could also account for the chemical composition of observed LMC PNe.

The collection of the SMC PNe observational data is presented in Section 2. In Section 3, we give the main physical and chemical input adopted to calculate the AGB evolutionary sequences used for the interpretation of the chemical composition in SMC PNe. The most relevant AGB evolutionary concepts are discussed in Section 4, while the comparison between models and observational data is given in Section 5. Section 6 describes the implications of this study for some of the most debated points regarding the AGB evolution. Finally, we summarize our conclusions in Section 7.

2 DATA SELECTION OF SMC PNe

PNe in the MCs have been observed for many decades, but it is only with the use of *Hubble Space Telescope* (*HST*) that we began to resolve them spatially, since they are about half an arcsecond in diameter. Once observed with the *HST*, compact H II regions at this distance are spatially resolved, and multiple stars that ionize the nebula are evident. We selected these compact H II regions out of our PN sample, since contamination of the PN sample with H II regions would be misleading for the comparison with AGB stellar evolution models that we are endeavouring. It turns out that it is even more likely to misclassify PNe in a low-metallicity ambient such as the SMC than in other environments (Stanghellini et al. 2003a).

The observational sample analysed in this paper and presented in Table 1 includes all and only the *HST* observed and spectroscopically confirmed SMC PNe, whose at least one abundances among those of He, C, N, O, Ne is known. In column (1) of Table 1, we list the usual name of the PN, where J, MA, MG, SMP, and SP indicate the original discovery or listing catalogues, with J referring to Jacoby (1980), MA to Meyssonnier & Azzopardi (1993), MG to Morgan & Good (1985), SMP to Sanduleak, MacConnell & Philip (1978), and SP to Sanduleak & Pesch (1981). Note that in some cases they may be listed in two or more catalogues, and we use the most commonly used names.

Column (2) lists the PN morphological class. All morphological types are based on *HST* observations, either using FOC or PC1 (SMP 03, SMP 05, SMP 10, SMP 15, SMP 16, SMP 21; Stanghellini et al. 1999) or STIS (Stanghellini et al. 2003a) images. Morphologies derived from STIS images were preferred when both STIS and one of the pre-refurbishment images were available. The morphological codes used in Table 1 have the following meanings: R is for Round, E for elliptical, EBC or RBC for round or elliptical with a bipolar core, and B for bipolar PNe. In some cases, round or elliptical PNe have some inner structure (Es) or an attached outer halo (ah), as indicated in the table. Unresolved PNe are indicated with U.

Columns (3) through (7) of Table 1 give the nebular abundances, in the usual terms of $(X/H) = \log(X/H) + 12$. Column (8) gives the references to the abundances, the first (or only) entry refers to ground-based abundances (He, N, O, Ne) while the second entry, if present, refers to carbon abundances, which is observed from space-based telescopes. All major recombination lines of carbon that are typically observed in PNe fall into the UV regime, thus its total abundance is only quantifiable via space observations, and thus harder to come by. It is worth noting that Shaw et al. (2010) calculated helium abundances with a method by Porter et al. (2005), but soon after the publication of the Shaw et al. (2010) paper, another prescriptions by Porter et al. (2005) had become available, and an erratum was published. To be on the safe side, where the helium emission lines were available from Shaw et al. (2010), we preferred to recalculate them with the prescription by Benjamin et al. (1999) to make the data set homogeneous.

The last two columns of Table 1 give the dust type of the PNe, and the relative reference. These types have been derived from *Spitzer* IRS spectra in the 4–38 μm range (Stanghellini et al. 2007, and Bernard-Salas et al. 2008). For the scope of this paper, it is sufficient to know whether the dust present in the PN has C-rich features, O-rich features, or it is featureless (F), as noted in the table.

Unless otherwise stated, we use the data of Table 1 for all the models-data comparison discussion and plots in this paper.

Table 1. SMC PN data.

Name (1)	Morph. (2)	(He/H) (3)	(C/H) (4)	(N/H) (5)	(O/H) (6)	(Ne/H) (7)	Ab. ref.[a] (8)	Dust type (9)	Dust ref.[b] (10)
J 04	E	11.02	–	8.04	7.30	6.76	SRM	–	–
J 18	R[c]	10.30	–	8.04	7.17	6.67	SRM	–	–
J 23	U	11.03	–	–	6.33	6.96	SRM	–	–
J 27	B[c]	–	–	7.97	7.86	–	KJ	–	–
MA 1682	B	11.19	–	–	7.40	7.34	SRM	–	–
MA 1762	EBC	10.93	–	–	7.29	6.39	SRM	–	–
MG 08	Es	11.08	–	7.15	8.15	6.39	S10[d]	–	–
MG 13	Es	10.94	–	5.12	8.00	7.12	S10[d]	–	–
SMP 1	U	10.83	–	7.16	7.86	6.42	LD	C-rich	BS09
SMP 2	R	11.11	8.74	7.47	8.01	7.21	LD, LDL	C-rich	S07
SMP 3	B	10.94	8.77	7.00	7.98	7.00	LD, LD	C-rich	BS09
SMP 5	R	11.11	8.90	–	8.24	–	LD, LDL	C-rich	S07
SMP 6	E	10.95	8.35	7.71	8.24	7.38	LD96, S09	C-rich	BS09
SMP 8	R	11.03	8.12	7.05	7.88	7.37	S10[d], S09	F	S07
SMP 9	Rs	10.85	8.79	7.25	8.32	7.51	S10[d], LD	F	S07
SMP 10	B	10.85	9.82[e]	7.82	8.58	7.65	LD, LD96	–	–
SMP 11	B	11.16	–	6.52	8.02	6.90	S10[d]	C-rich	BS09
SMP 12	E	11.01	–	–	–	6.89	LD	–	–
SMP 13	R	11.05	8.73	7.30	8.06	7.35	S10[d], S09	C-rich	S07
SMP 14	R	10.94	–	7.36	8.29	7.65	S10[d], LD	C-rich	S07
SMP 15	R	11.14	8.26	7.38	8.21	7.67	LDL, S09	C-rich	S07
SMP 16	E	10.69	8.19	6.55	7.85	6.37	LD, S09	C-rich	S07
SMP 17	R(ah)	11.05	8.40	7.50	8.24	7.58	S10[d], LDL	C-rich	S07
SMP 18	U	11.04	8.31	7.11	7.90	7.57	S10[d], S09	C-rich	S07
SMP 19	R	11.00	8.97	7.28	8.14	7.63	S10[d], LD	C-rich	S07
SMP 20	U	11.07	8.25	6.95	7.74	6.91	S10[d], S09	C-rich	S07
SMP 21	Es	11.00	7.13	7.92	7.55	6.84	LD, LD96	–	–
SMP 22	B[c]	11.07	7.23	8.05	7.59	6.72	LD96, LD	F	BS09
SMP 23	EBC	11.00	8.39	7.24	7.93	7.37	S10[d], LD	F	S07
SMP 24	E	11.04	8.18	7.17	8.06	7.36	S10[d], S09	C-rich	BS09
SMP 25	E	11.02	6.64	7.92	7.56	6.96	LD, S09	O-rich	S07
SMP 26	P	10.96	8.46	8.10	8.14	7.43	LD, S09	F	S07
SMP 27	R(ah)	11.04	–	7.17	8.00	7.20	S10[d]	C-rich	S07
SMP 28	E	11.11	6.96	8.04	7.46	6.85	LD96, S09	F	BS09
SP 34	R(ah)	10.86	–	7.30	7.82	7.05	SRM	–	–

Table reference notes. [a]Abundance reference keys: KJ (Kaler & Jacoby 1980); LD (Leisy & Dennefeld 2006); LD96 (Leisy & Dennefeld 1996); LDL are from LD96 with lines from the literature cited therein; S10 (Shaw et al. 2010); SRM (Stasińska, Richer & McCall 1988); S09 (Stanghellini et al. 2009). [b]Dust references keys: BS09 (Bernard-Salas et al. 2009); S07 (Stanghellini et al. 2007). [c]Uncertain morphology. [d](He/H) recalculated from S10 emission lines and Benjamin et al. (1999) prescription (see text). [e]Uncertain abundance.

3 MODELLING AGB EVOLUTION AND DUST FORMATION

3.1 Stellar evolution models

The evolutionary sequences used in this work were calculated with the ATON code; an interested reader can find the details of the numerical and physical structure of the code in Ventura et al. (1998), whereas the most recent updates are presented in Ventura & D'Antona (2009).

The ingredients used most relevant for the present investigation are the following:

(i) *Chemical composition*. The AGB models are calculated in the mass range $0.8\,M_\odot \leq M \leq 8\,M_\odot$[1] and for the metallicities $Z = 1$, 2, 4, 8×10^{-3}. The mixture adopted is taken from Grevesse & Sauval (1998). In agreement with our previous investigations, for the $Z = 1$, 2×10^{-3} models, we used an α-enhancement $[\alpha/\mathrm{Fe}] = +0.4$, whereas for the higher Z models we used $[\alpha/\mathrm{Fe}] = +0.2$; in the interpretation of the results, we will take into account that the best choice for the SMC stars would be a solar-scaled or even subsolar distribution of α elements. A few test models with $[\alpha/\mathrm{Fe}] = -0.2$ for the $Z = 2 \times 10^{-3}$ metallicity were calculated. The initial chemical composition for the four sets of models used here is reported in Table 2, in terms of the CNO elements and of helium.

Table 2. Initial chemical composition of the AGB models.

Z	(He/H)	(C/H)	(N/H)	(O/H)	(Ne/H)
10^{-3}	11.52	8.05	7.52	8.89	8.23
2×10^{-3}	11.52	8.35	7.82	9.19	8.53
4×10^{-3}	11.55	8.82	8.29	9.46	8.80
8×10^{-3}	11.55	9.13	8.60	9.76	9.11

(ii) *Convection.* The temperature gradient within regions unstable to convective motions is found by means of the full spectrum of turbulence (FST) model (Canuto & Mazzitelli 1991). Nuclear

[1] The upper limit to the AGB evolution is indeed slightly dependent on the metallicity. For low-metallicity models, i.e. $Z = 1$, 2×10^{-3}, the highest mass considered is $7.5\,M_\odot$. Models with mass $M \geq 7\,M_\odot$ develop a core composed of oxygen and neon.

burning and mixing of chemicals are coupled in a diffusive-like scheme (Cloutmann & Eoll 1976). During the AGB phase, overshoot of convective eddies from the bottom of the envelope and from the top and bottom borders of the shell which forms at the ignition of each thermal pulse, is described by means of an exponential decay of velocities from the convective/radiative interface, fixed by the Schwarzschild criterion. The e-folding distance is assumed to be $0.002H_{\rm p}$ (where $H_{\rm p}$ is the pressure scaleheight calculated at the formal boundary of convection), in agreement with the calibration based on the observed luminosity function of carbon stars in the LMC, given by Ventura et al. (2014b).

(iii) *Mass-loss.* The mass-loss rate for oxygen-rich models is determined via the Blöcker (1995) treatment; following the calibration based on the luminosity function of carbon stars in the LMC by Ventura, D'Antona & Mazzitelli (2000), we set the free parameter entering the Blöcker (1995) recipe to $\eta_R = 0.02$. For C/O > 1 environments, we used the results from the Berlin group (Wachter et al. 2002, 2008).

(iv) *Molecular opacities.* The molecular opacities in the low-temperature regime (below 10^4 K) are calculated by means of the AESOPUS tool (Marigo & Aringer 2009). The opacities are suitably constructed to follow the changes in the chemical composition of the envelope, particularly of the individual abundances of carbon, nitrogen, and oxygen.

3.2 Dust formation in the winds of AGB stars

The formation and growth of dust particles in the wind of AGB stars is described by means of the pioneering scheme described by the Heidelberg group (Ferrarotti & Gail 2006). All the relevant equations, with a detailed explanation of the physical assumptions adopted, can be found in Ferrarotti & Gail (2006) and in the series of papers on this argument published by our group (Ventura et al. 2012a,b; Di Criscienzo et al. 2013; Ventura et al. 2014b).

The wind is assumed to expand isotropically from the surface of the star. Mass and momentum conservation allows the determination of the radial profiles of density and velocity. The effects of dust on the dynamics of the wind is described by the extinction coefficient, k, which is used to calculate the radiation pressure and the consequent acceleration of the wind; this quantity depends on the number density and size of dust grains formed (equations 2 and 9 in Ferrarotti & Gail 2006).

The dust species formed depend on the chemical composition of the surface layers of the stars, primarily on the C/O ratio. For oxygen-rich environments, we consider the formation of silicates and alumina dust, whereas in the wind of carbon stars we account for the formation of solid carbon and silicon carbide. The rate of the grain growth is found on the basis of the values of density and of the mass fraction of the chemical elements relevant for the formation of the various dust species, namely silicon (silicates and silicon carbide), aluminium (alumina dust), and carbon (solid carbon).

The formation of dust has a direct influence on the AGB evolution, because it favours the acceleration of the wind, thus an increase of the rate with which mass is lost from the envelope.

4 THE AGB EVOLUTION

The models presented here are extensively illustrated and discussed in Ventura et al. (2014a, $Z = 4 \times 10^{-3}$), Ventura et al. (2013, $Z = 1$, 8×10^{-3}, initial mass above $3\,{\rm M}_{\odot}$), and Ventura et al. (2014b, low-mass models of metallicity $Z = 1$, 8×10^{-3} and initial mass below $3\,{\rm M}_{\odot}$). The models are the same used in Paper I, with the only exception of the $Z = 2 \times 10^{-3}$ evolutionary sequences, which were calculated specifically for the present investigation.

The evolution of the surface chemical composition of AGB stars is known to be driven by the combined effects of TDU and HBB (Karakas & Lattanzio 2014). The former favours an increase in the surface carbon and, in smaller quantities, of the oxygen content. HBB provokes the change in the relative fractions of the CNO elements, according to the equilibrium determined by the temperature at the base of the convective envelope. The surface carbon is destroyed in favour of nitrogen; for temperatures above ∼80 MK oxygen depletion occurs. TDU is the dominant mechanism for stars of initial mass below $\sim 3\,{\rm M}_{\odot}$, whereas the effects of HBB prevail in the high-mass regime (see, e.g. Ventura et al. 2013).

Fig. 1 shows the evolution of $Z = 2 \times 10^{-3}$ models of different mass in terms of the individual mass fractions of carbon, nitrogen, and oxygen. Similar plots for the other metallicities were shown in Paper I. To allow the simultaneous plot of all the evolutionary sequences, we use the stellar mass as abscissa instead of the AGB time; the individual sequences must be read rightwards, as mass diminishes during the evolution. The models shown in the figure can be considered as representative of the different behaviours.

(i) Stars of mass below $\sim 3\,{\rm M}_{\odot}$ (represented by the $2\,{\rm M}_{\odot}$ model in Fig. 1) do not experience any HBB; consequently, the variation of the chemical composition is entirely determined by TDU. For stars of initial mass above $\sim 0.9\,{\rm M}_{\odot}$, the final chemistry is enhanced in carbon and, in more modest quantities, in oxygen: these stars reach the carbon-star stage during the AGB evolution and end up their life with a surface C/O above unity. The nitrogen content is changed after the first dredge-up episode during the red giant branch phase and remains practically unchanged for the whole AGB phase. Among the stars belonging to this group, the model shown in Fig. 1 is one of those undergoing the greatest variation of the surface chemical composition, as result of the effect of several TDU events; in models of smaller mass, the increase in the carbon and oxygen content is smaller.

(ii) The chemical composition of stars of mass $3\,{\rm M}_{\odot} < M < 4\,{\rm M}_{\odot}$ is affected by both TDU and HBB. These objects are the most efficient manufactures of nitrogen, because the latter species is produced not only by the carbon initially present in the envelope, but also by the additional carbon dredge-up after each thermal pulse. In Fig. 1, this class of objects is represented by the $3\,{\rm M}_{\odot}$ model. The variation of the surface carbon is the most indicative of the balance between TDU and HBB: the increase of C in the initial phases are a consequence of TDU, whereas the following depletion of carbon is due to the HBB activity. In the very final AGB phases, when HBB is extinguished, the C-star stage can be achieved.

(iii) HBB is the dominant mechanism in changing the surface chemistry of stars with mass in the range $4\,{\rm M}_{\odot} < M < 6\,{\rm M}_{\odot}$. However, these objects are also expected to experience a few TDU episodes towards the end of the AGB evolution, when HBB is extinguished. These stars are efficient nitrogen producers, whereas their carbon and oxygen content is smaller compared to the initial abundance. The final carbon content depends on the number of TDU episodes experienced during the latest thermal pulses. In Fig. 1, we represent this group of stars by showing the evolution of a $4.5\,{\rm M}_{\odot}$ model. The effects of HBB can be seen in the initial decrease in the surface carbon and in the drop in the carbon mass fraction which follow each thermal pulse, after the increase due to TDU.

(iv) The chemical composition of massive AGB stars, with mass $M > 6\,{\rm M}_{\odot}$, reflects the pure effect of HBB. The overall effect of

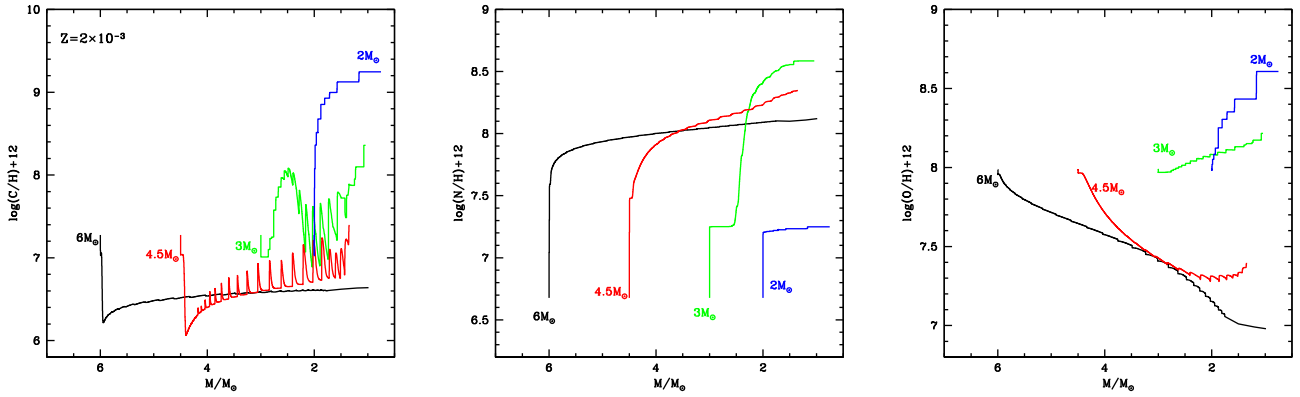

Figure 1. The evolution of the surface mass fraction of carbon (left), nitrogen (middle), and oxygen (right) during the AGB phase of models of metallicity $Z = 2 \times 10^{-3}$ and of initial masses 2, 3, 4.5, and 6 $M_{\odot}$.

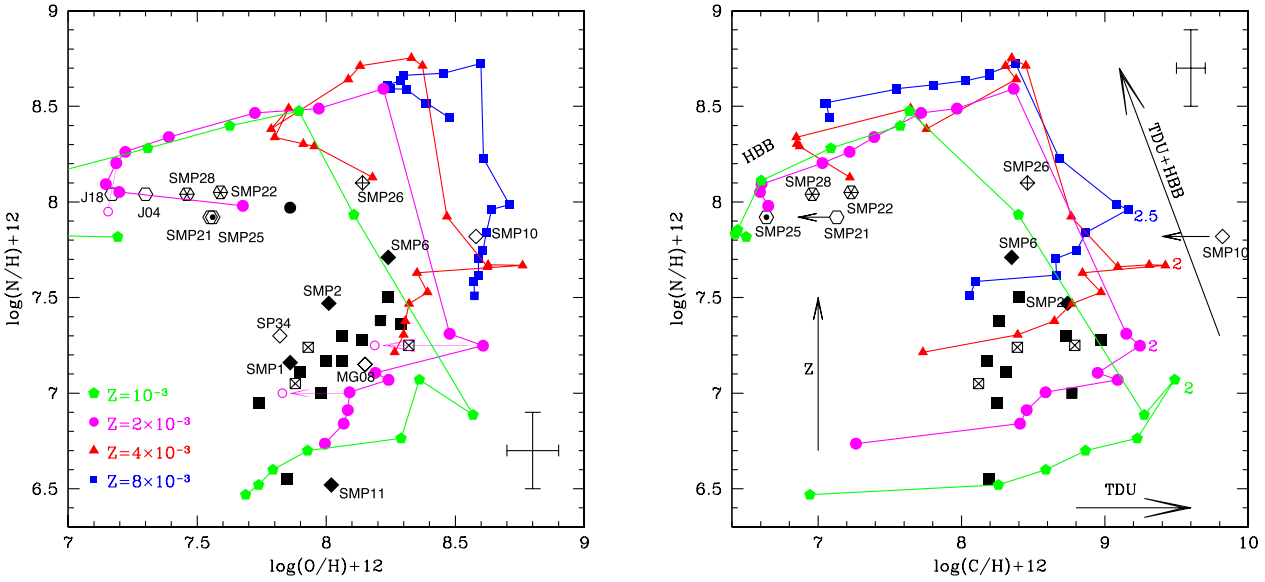

Figure 2. The observed chemical composition of the SMC PNe sample in the O–N (left-hand panel) and C–N (right) planes. Squares, hexagons, and diamonds indicate the loci of PNe, respectively, of groups (a), (b), and (c) [see Section 5]. Filled symbols mark PNe with traces of carbon dust, open-dotted symbols indicate evidence of silicates, open symbols indicate PNe with no indication of dust in the literature, and crossed symbols indicate featureless IRS spectra. We indicate the PN names for groups (b) and (c) PNe. Typical errors associated with the determination of the abundances of the individual species are indicated with crosses in the right, bottom side of the left-hand panel and in the right, top region of the right-hand panel. The final abundances of the AGB models of metallicity $Z = 10^{-3}$ (green pentagons), $Z = 2 \times 10^{-3}$ (magenta circles), $Z = 4 \times 10^{-3}$ (red triangles), and $Z = 8 \times 10^{-3}$ (blue squares) are also shown (see legend in the O–N plot). Open, magenta circles in the left-hand panel refer to $Z = 2 \times 10^{-3}$ models calculated with a lower initial oxygen ([O/Fe] = −0.2).

the nuclear activity at the bottom of the convective envelope is the reduction of the surface carbon and oxygen, and the increase in the nitrogen mass fraction; the overall C+N+O content is unchanged. The 6 $M_{\odot}$ model in Fig. 1 was chosen as a representative of this class of objects. The effects of HBB can be seen in the initial drop in the surface carbon and in the decrease in the surface oxygen, which occurs in the following evolutionary phases. Note that the surface oxygen is much more sensitive than carbon to the temperature at which HBB occurs: looking at the 6 $M_{\odot}$ tracks in Fig. 1, we see that while the oxygen decrease continues during the whole AGB phase, as a consequence of the higher HBB temperatures, the surface carbon, after the initial decrease, keeps approximately constant.

The range of masses of the four groups given above are slightly dependent on the metallicity of the models. This holds in particular for the first and the second group, because HBB is activated more easily in stars of lower metallicity: therefore, the upper limit of the mass of the stars experiencing solely TDU changes from ∼3 $M_{\odot}$ for $Z = 4, 8 \times 10^{-3}$, down to ∼2.5 $M_{\odot}$ for $Z = 1, 2 \times 10^{-3}$. Concerning group (iv), the highest mass not undergoing core collapse is ∼8 $M_{\odot}$ for $Z = 4, 8 \times 10^{-3}$, whereas it is ∼7.5 $M_{\odot}$ for $Z = 1, 2 \times 10^{-3}$.

The final chemical composition of the various models used in this work are shown in Fig. 2, in the C versus N and O versus N planes. Tracks of different colours connect models of different metallicity and different masses in the range $0.9\,M_{\odot} < M < 8\,M_{\odot}$, where masses increase counter-clockwise for each metallicity track. In the low-mass regime, corresponding to the stars discussed in point (i) above, the final carbon and oxygen increase with the initial mass of the star, because more massive objects undergo a higher number of TDU events. The trend in both planes is reversed for masses around 3 $M_{\odot}$ [point (ii) above], because HBB sets in determining the increase in the surface nitrogen and a partial destruction of the

carbon accumulated by TDU. In the higher mass domain [points (iii) and (iv) above], the theoretical sequences gradually move to the left-upper regions of the diagrams, those corresponding to a chemical composition entirely determined by the equilibria of HBB.

The metallicity of the star affects the final chemical composition owing to the difference in the initial mass fractions of the relevant dust species, and to the sensitivity of some of the mechanisms able to alter the surface chemical composition to the metal content of the star. We stress here the following two main effects of metallicity.

(i) In the low-mass domain, the chemical species mostly affected by changes in the metallicity is nitrogen. The final N of these objects is solely determined by the first dredge-up event, taking place during the red giant branch evolution. Therefore, a spread in the metallicity of the stars will reflect into a spread in the surface N.

(ii) Concerning massive AGBs, the stars of smaller metallicity undergo stronger HBB, with higher temperatures at the base of the convective envelope (Ventura et al. 2013); therefore, low-Z models experience a more advanced nucleosynthesis. This will reflect essentially in a smaller oxygen, because the higher temperatures lead to a more efficient activation of the full CNO cycling; conversely, in higher Z model, little depletion of oxygen occurs. In agreement with the arguments of point (iv) before, we find that the final oxygen is the best metallicity indicator in these stars. This is because carbon burning requires smaller temperatures, thus it is activated in models of all metallicities; furthermore, the carbon equilibrium abundance is not very sensitive to the temperatures at which HBB occurs, once the minimum threshold required to ignite HBB, i.e. $T \sim 40$ MK, is reached.

5 PLANETARY NEBULAE IN THE SMC

In order to interpret each PN in our sample to the evolutionary path that lead to the observed configuration, we use the comparison between the nebular abundances and the AGB yields of the final ejected envelopes. In the panels of Fig. 2, we show the data points in black, and the model points in colours. The final abundances of the AGB models of different initial metallicity, given in Table 2, are given by different symbols and colours (see the legend on the left-hand panel). The left-hand panel, showing N versus O abundances, and the right-hand panel, showing N versus C abundances, show that models encompass well the observed PNe. Before we describe in detail the different PN groups of Fig. 2, let us examine closely the metallicity dependence of the various populations.

In Fig. 2, left-hand panel, there is a notable sequence of PNe where N and O are almost correlated. To further investigate the relationship between nitrogen and the metallicity, we show the N against Ne trend in Fig. 3. We prefer neon to argon and sulphur as metallicity indicator of the PNe progenitors, because the neon abundance is available for all but two of the PNe considered here and, more important, the errors associated with the measurements of neon are significantly smaller in comparison to argon and sulphur (Leisy & Dennefeld 2006). An additional reason to disregard sulphur is the well-known 'sulphur anomaly' (Henry et al. 2012); e.g. it may even be depleted into dust (Pottasch & Bernard-Salas 2006). The only problem with using neon as metallicity indicator is that the surface abundance of this chemical species can be changed during the AGB phase: however, as shown in Fig. 4, the only significant changes, at most by a factor ∼3, are obtained in stars in a narrow range of mass around ∼2 $M_\odot$ (i.e. those undergoing the most relevant modification via TDU). To further test the relationship between nitrogen and metallicity, we checked the argon–nitrogen

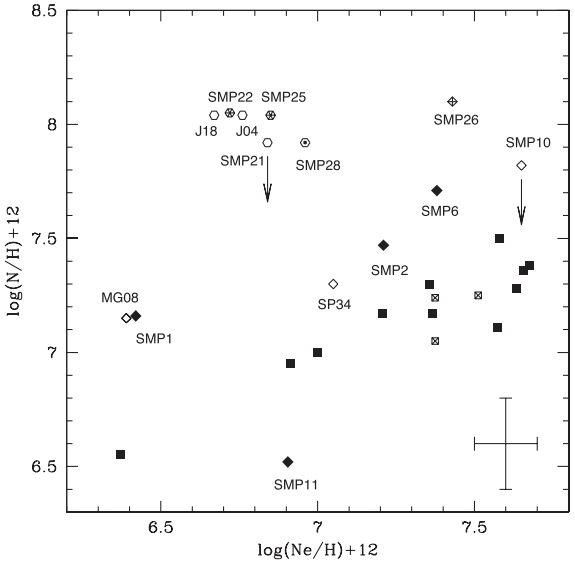

Figure 3. The nitrogen abundances of the PNe sample introduced in Section 2 as a function of their neon content. The symbols are the same as in Fig. 2. The cross in the right, lower part of the plane gives the typical errors in the neon and nitrogen abundances.

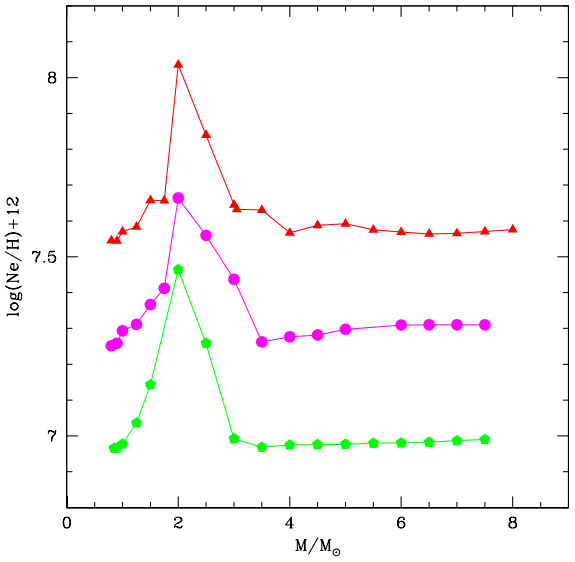

Figure 4. The final neon abundance of the models used in this analysis as a function of the initial mass. The metallicities $Z = 10^{-3}$, $Z = 2 \times 10^{-3}$, and $Z = 4 \times 10^{-3}$ are indicated, respectively, with green pentagons, magenta circles, and red triangles. The initial abundances of neon for the three cases are $\log(\mathrm{Ne/H}) + 12 = 6.93$ ($Z = 10^{-3}$), $\log(\mathrm{Ne/H}) + 12 = 7.24$ ($Z = 2 \times 10^{-3}$), and $\log(Ne/H) + 12 = 7.51$ ($Z = 4 \times 10^{-3}$).

trend and verified that it follows the same behaviour, though with a higher dispersion, as the Ne–N relationship.

The majority of PNe in Fig. 3 follows an approximately linear Ne–N trend, indicating that N increases with metallicity; we will refer to this PN sequence as group (a) in the following, and plot them with square symbols in the figures. Notably displaced from the sequence, with large-enhanced nitrogen, there is a smaller group of PNe which we plot with hexagons in the figures and refer as group (b). Finally, we can identify another minor group of PNe, indicated with diamonds in the figures, whose position in the plane deviates slightly (more than 0.3 dex) from the main N–Ne trend traced by

group (a) PNe. We will refer to this subsample as group (c). All the PNe in group (a) and (c) exhibit C/O ratios above unity.

5.1 Carbon-rich PNe

In the right-hand panel of Fig. 2, we see that all group (a) PNe, indicated with squares, have enhanced carbon. We interpret these PNe as the progeny of stars of mass $M < 2\,M_{\odot}$. The observed spread in N of group (a) PNe is due to differences in the progenitor's metallicity of these objects, as clearly shown in Fig. 3. Most of these PNe descend from $\sim$1–1.5 $M_{\odot}$ stars of metallicity in the range $2 \times 10^{-3} < Z < 4 \times 10^{-3}$, formed between 1.5 and 7 Gyr ago. PNe with $\log(C/H) + 12 > 8.5$ can be interpreted as the final phases of stars of higher mass ($\sim$2–2.5 $M_{\odot}$), formed in more recent epochs, 0.5–1 Gyr ago. The models nicely reproduce the observed spread in carbon; the only exception is PN SMP 10, where only upper limit carbon abundance is available in the literature (Leisy & Dennefeld 2006). The *Spitzer* IR spectra of most group (a) SMC PNe exhibit C-rich dust features, indicated with filled symbols in the plots. This is consistent with the evolution through the C-rich phase, already noted by Stanghellini et al. (2007). Conversely, no PN with traces of O-rich dust in their *Spitzer* spectra is found in group (a).

Oxygen abundances of group (a) PNe show a considerable offset to lower abundances with respect to the $Z = 2$–4×10^{-3} models (left-hand panel of Fig. 2), indicating that the original composition of SMC interstellar material is oxygen-poor with respect to what has been assumed for the models (see Table 2). This is confirmed by a few test $Z = 2 \times 10^{-3}$ models, calculated with a lower O mixture, that nicely reproduce several of the observed points of group (a). This result is not surprising, given the low oxygen abundances detected in F supergiant stars in the SMC (Spite, Barbuy & Spite 1989) and the chemical and structural evolutionary models for the SMC, which predict lower oxygen for stars in the SMC, compared to objects of the same metallicity in the LMC and in the Milky Way (Russell & Dopita 1992).

5.2 PNe enriched in nitrogen: the signature of HBB

PNe in group (b) are indicated with Hexagons in Figs 2 and 3. Their surface chemical composition shows the signature of HBB: this is clearly visible in the enhancement of nitrogen and in the low abundances of carbon and oxygen. The analysis of their loci on the CN plane (Fig. 2, right-hand panel) supports the idea that these PNe descend from massive AGB stars, whose metallicity is in the range $10^{-3} < Z < 4 \times 10^{-3}$. The ON plane, for the reasons given at the end of the previous section, allows a better discrimination among the various metallicities, suggesting that only low-Z models are compatible with the observed abundances of oxygen. We conclude that PNe in group (b) are the progeny of low-metallicity stars of mass $6\,M_{\odot} < M < 7.5\,M_{\odot}$, formed 40–70 Myr ago. The chemical composition of these stars is not affected by TDU; this confirms the possibility, outlined in Paper I, that the chemistry of massive AGB stars shows the sole chemical imprinting of HBB, with no contamination from TDU. Note that this conclusions still holds if we consider models with lower initial oxygen abundance. This is shown in the left-hand panel of Fig. 2, where we compare the PNe with a $6\,M_{\odot}$ model of metallicity $Z = 2 \times 10^{-3}$, calculated with an [O/Fe] $= -0.2$ mixture. Compared to the $6\,M_{\odot}$, [O/Fe] $= +0.2$ model, the main difference is that the final N is a factor of $\sim$2 lower (note that this is in better agreement with the data of group (b) PNe), whereas the final O is only slightly ($\sim$0.1 dex) less abundant. This is because the [O/Fe] $= -0.2$ model has a smaller, initial C+N+O and, under HBB conditions, N is the main product of the nucleosynthesis activated.

Apart from SMP 21, whose carbon abundance is an upper limit and very unreliable, there are three clear members of group (b): SMP 22, SMP 25, and SMP 28. Interestingly, SMP 25 is the only PN in the SMC that has been detected to have O-rich dust, and this is perfectly compatible with having a higher mass progenitor, as derived from the comparison with the tracks. The other two PNe have also *Spitzer* spectra available, with F dust spectra, which typically means that their dust has sputtered by the time of observations (Stanghellini et al. 2007). This is also consistent with a higher mass progenitor and a generally rapid shell evolution.

While on a pure chemical point of view, the possibility that PNe in group (b) descend from massive AGB progenitors is in nice agreement with the observations, statistical arguments are at odds with the hypothesis that such a large ($\sim$18 per cent) fraction of the PNe in the sample are the progeny of high-mass AGB stars. The short post-AGB lifetimes of stars with core mass above 0.9 $M_{\odot}$ ($\sim$60 yr, Bloecker 1995) and the relatively small percentage of stars with mass in the range 6–8 $M_{\odot}$ expected on the basis of any realistic mass function are marginally compatible with the possibility that 6 out of 35 PNe descend from massive AGB progenitors.

Part of group (b) PNe might descend from low-mass stars of initial mass below $\sim$1.25 $M_{\odot}$ (thus not becoming C stars), which experienced some non-standard mixing during the previous giant branch phases, thus enriching the surface layers in N-rich and C-poor material. This hypothesis is supported by results showing that stars of mass below $\sim$2 $M_{\odot}$ experience deep mixing during the ascent of the first giant branch (Gilroy 1989, 1991; Angelou et al. 2012). For half of the stars in this group, the low oxygen abundances measured are compatible with low-metallicity progenitors, if a 0.2 dex error bar is assumed.

A further possibility is that some PNe in group (b) belong to binary systems composed of low-mass stars, which evolved through a common envelope phase at the tip of the RGB or during the early AGB phase; these systems would show the imprinting of CN cycling, avoiding the achievement of the C-star phase. On the statistical side, this evolutionary scenario is plausible, given that $\sim$50 per cent of stars with mass above 1 $M_{\odot}$ are part of binary systems.

5.3 A few outliers

Group (c) PNe, plotted with diamonds in the figures, exhibit anomalous nitrogen abundances, falling off the main N–Ne locus in Fig. 3. PNe SMP 1, SMP 2, SMP 11, SP 34, and MG 8 populate the region in the ON plane reproduced by low-mass stars models (see left-hand panel of Fig. 2), which became carbon stars after experiencing a few thermal pulses. We are forced to base our analysis on this plane only, because the carbon abundance is available only for the source SMP 2. The N abundance is so small that any HBB effect can be disregarded. We conclude that their anomalous nitrogen is likely due to intrinsic fluctuations, probably originating by the poor precision of the nitrogen determinations compared to other elements (Leisy & Dennefeld 2006).

The position of SMP 6 in the ON and CN planes can be interpreted either as a high-metallicity PN with low-mass progenitor, which eventually became carbon star under the effects of TDU, or as the progeny of a low-metallicity star of mass $\sim$3 $M_{\odot}$, whose final surface chemistry reflects the effects of both TDU and HBB; the latter mechanism would be responsible for the unusually large

nitrogen observed. The large abundance of neon (see Fig. 3) would suggest the first hypothesis.

The nitrogen observed in SMP 26 is by far incompatible with low-mass stellar evolution, rather pointing towards a higher mass progenitor. The overall CNO abundances suggest that this object descends from a low-metallicity star with mass at the edge of HBB ignition: the carbon-star stage was reached as a consequence of several TDU episodes, whereas the high N was due to proton capture by some of the carbon nuclei transported to the surface.

6 PNe IN THE SMC: A FURTHER TEST FOR AGB MODELLING

The results presented here show that the majority of PNe in the SMC descend from low-mass progenitors, of initial mass below $2\,M_{\odot}$. This conclusion holds for all PNe in group (a) and for a large fraction of the outliers, those in group (c). On this aspect, the SMC is significantly different from the LMC. In fact, as shown in Paper I, the fraction of LMC PNe descending from stars of mass above $\sim 3\,M_{\odot}$ is significantly larger than that of SMC PNe. This result is however not surprising, if we consider the different star formation histories (SFH) experienced by the two galaxies. The LMC SFH has two prominent peaks at ∼100 and ∼500 Myr (Harris & Zaritsky 2009), which favoured the formation of stars of mass in the range 3–7 $M_{\odot}$; conversely, the SMC SFH presents a single, extremely narrow peak at ∼500 Myr (Harris & Zaritsky 2004), which is consistent with the progeny of the low-mass AGB stars observed.

The large majority of SMC PNe are carbon rich, with a C/O ratio above unity; this indicates that all these objects descend from stars that reached the C-star stage during the AGB evolution. Only a small minority of SMC PNe are C-poor (and N-enhanced). This further difference between the SMC and LMC PNe is explained by the average lower metallicity of SMC stars compared to those in the LMC. Naturally, carbon stars(C/O>1) at low metallicity (and lower oxygen) are favoured since a smaller amount of carbon needs to be dredged up to reach the critical condition that define them. Furthermore, the depth of TDU increases with decreasing metallicity (Boothroyd & Sachmann 1988), which enhances the surface carbon enrichment, thus the process goes in the same direction of favouring C stars in the SMC with respect to the LMC. The fact that the spectra of most of the SMC PNe observed presents the signature of carbon-rich dust adds more robustness to this interpretation.

The most significant source of uncertainty in the modelling of low-mass AGB stars is the extension of TDU, which drives the increase in the surface carbon. The efficiency of TDU depends on physical parameters, primarily the core mass and the metallicity. These dependences are still highly uncertain, which reflects our poor knowledge of how convection works in stars. Based on the comparison with the luminosity function of carbon stars in the MC, synthetic AGB models have been extensively used to calculate the core mass at which TDU begins and the extension of the mixed region (Groenewegen & de Jong 1993; Marigo, Girardi & Bressan 1999; Izzard et al. 2004). Detailed, standard models, where the convection/radiation interface is fixed via the Schwartzschild criterion, could not reproduce the observations (Karakas, Lattanzio & Pols 2002), thus suggesting that some overshoot from the base of the convective envelope is required. The need for some extra-mixing was invoked by Herwig et al. (2007), based on numerical simulations and, more recently, by Kamath, Karakas & Wood (2012), on the basis of the comparison between the observed and expected transition luminosity from O-rich to C-rich stars in clusters in the MC. Extra-mixing from the bottom of the envelope has been used in almost the totality of the most recent works on AGB modelling (Cristallo et al. 2009; Weiss & Ferguson 2009; Ventura et al. 2014b; García-Hernández et al. 2016).

The carbon abundance of the PNe discussed here is $\log(\mathrm{C/H}) + 12 < 9$ (see right-hand panel of Fig. 2), which falls within the range of the evolutionary models; the C/O ratios never exceed ∼7.

The PNe belonging to group (b) exhibit a chemical composition with the clear imprinting of CNO nucleosynthesis. While common envelope evolution in binary systems or non-standard mixing of low-mass stars could partly explain this group of stars (see discussion at the end of the previous section), it is likely that a few of these PNe have experienced HBB during the AGB evolution, which would explain the significant nitrogen enhancement and the low carbon and oxygen abundances measured. This would suggest massive progenitors, evolving on core masses above $\sim 0.9\,M_{\odot}$ (Ventura et al. 2013). For stars in this mass domain, convection is once more the major uncertainty, for two reasons: (a) the efficiency of convection determines the temperature at the base of the envelope (Ventura & D'Antona 2005), which is particularly relevant for the evolution of the surface oxygen; (b) the possible occurrence of TDU, still debated, would eventually increase the surface carbon, and, in some cases, produce high-luminosity carbon stars (Frost et al. 1998).

The surface chemical composition of group (b) PNe is nicely reproduced by our massive AGB models of metallicity $Z = 2 \times 10^{-3}$. This result, if confirmed, would be the most reliable confirmation obtained so far that low-metallicity AGB stars of mass $M > 6\,M_{\odot}$ undergo a very advanced nucleosynthesis at the base of their envelope, as a result of HBB temperatures above ∼80 MK. This finding indicates that envelope convection is highly efficient in low-metallicity, massive AGB stars, as predicted by the FST schematization adopted here. Note that a similar result can be obtained within the traditional mixing-length theory description, provided that a mixing length significantly higher than the standard vale used to reproduce the evolution of the Sun is adopted (Doherty et al. 2014). Furthermore, the extremely low carbon abundances measured in these stars indicate that TDU has negligible (if any) effects on the evolution of the surface chemistry of these objects, at odds with other models for stars of similar mass and metallicity, which predict much higher quantities of carbon (see Fishlock et al. 2014 and references therein).

7 CONCLUSIONS

We characterize the PNe population of the SMC based on AGB models of various mass and metallicity, which account for dust production in the circumstellar envelope.

We found that most of the PNe in the observed sample descend from stars with mass in the range $1\,M_{\odot} < M < 2\,M_{\odot}$ and metallicity $Z \sim 2$–4×10^{-3}, formed between 1 and 7 Gyr ago. Unlike their counterparts in the LMC, all SMC PNe have measured C/O ratio above unity; this is consistent with the evolutionary models, according to which the achievement of the C-star stage is easier in stars of lower metallicity, as those currently evolving to PNe in the SMC. The analysis of the observed oxygen abundances, compared to the models, outlines that SMC PN progenitors formed out of a medium that was poorer in oxygen than the medium at the time of LMC PN progenitor formation, and that of the Milky Way. This is in agreement with the studies focused on the chemical evolution of the SMC.

The spread in carbon abundances observed in SMC PNe is nicely reproduced by the AGB models; this adds more robustness to the models used in the present investigation, particularly for what concerns the depth of the TDU experienced.

Six PNe in the SMC sample are greatly enhanced in nitrogen, thus indicating some CN (or CNO) activity. The chemical composition of these objects is reproduced by low-metallicity stars of initial mass close to the threshold limit to undergo core collapse. Deep mixing during the red giant branch, common envelope evolution, and binarity are additional possibilities for this chemistry. While for reasons related to the mass function and to the relatively short duration of the post-AGB phase of these objects, it seems unlikely that all these stars descend from massive AGB progenitors, it is reasonable to believe that part of these systems are the progeny of stars of mass in the range $6\,M_{\odot} < M < 8\,M_{\odot}$ and metallicity $Z \sim 4$–8×10^{-3}. The overall CNO chemistry of these PNe traces the equilibria of advanced HBB nucleosynthesis, corresponding to temperatures at the base of the convective envelope of the order of ∼100 MK. If this hypothesis is confirmed, it would provide a strong indication that in low-metallicity, massive AGB stars, convection is highly efficient. In four out of the six sources, the carbon abundance is extremely small, thus indicating negligible effects of TDU.

We have now compared the best observed PN sample of the MCs to the AGB stellar evolutionary models of adequate metallicity. In the future, we plan a similar study extended to Galactic PNe to increase the metallicity baseline of the comparison.

ACKNOWLEDGEMENTS

MDC acknowledges the contribution of the FP7 SPACE project ASTRODEEP (Ref.No:312725), supported by the European Commission. DAGH was funded by the Ramón y Cajal fellowship number RYC−2013−14182 and he acknowledges support provided by the Spanish Ministry of Economy and Competitiveness (MINECO) under grant AYA−2014−58082-P. FD acknowledges support from the Observatory of Rome.

REFERENCES

Angelou G. C., Stancliffe R. J., Church R. P., Lattanzio J. C., Smith G. H., 2012, ApJ, 749, 128
Benjamin R. A., Skillman E. D., Evan D., Smits D. P., 1999, ApJ, 514, 307
Bernard-Salas J., Peeters E., Sloan G. C., Gutenkunst S., Matsuura M., Tielens A. G. G. M., Zijlstra A. A., Houck J. R., 2009, ApJ, 699, 1541
Bernard-Salas J., Pottasch S. R., Gutenkunst S., Morris P. W., Houck J. R., 2008, ApJ, 672, 274
Blöcker T., 1995, A&A, 297, 727
Blöcker T., Schöenberner D., 1991, A&A, 244, L43
Bloecker T., 1995, A&A, 299, 755
Boothroyd A. I, Sachmann I.-J., 1988, ApJ, 328, 653
Boyer M. L. et al., 2011, AJ, 142, 103
Boyer M. L. et al., 2012, ApJ, 748, 40
Canuto V. M. C., Mazzitelli I., 1991, ApJ, 370, 295
Cioni M. R. L., van der Marel R. P., Loup C., Habing K. J., 2000, A&A, 359, 601
Cloutmann L., Eoll J. G., 1976, ApJ, 206, 548
Cristallo S., Straniero O., Gallino R., Piersanti L., Dominguez I., Lederer M. T., 2009, ApJ, 696, 797
Dell'Agli F., Ventura P., García-Hernández D. A., Schneider R., Di Criscienzo M., Brocato E., D'Antona F., Rossi C., 2014, MNRAS, 442, L38
Dell'Agli F., Ventura P., Schneider R., Di Criscienzo M., García-Hernández D. A., Rossi C., Brocato E., 2015a, MNRAS, 447, 2992
Dell'Agli F., García-Hernández D. A., Ventura P., Schneider R., Di Criscienzo M., Rossi C., 2015b, MNRAS, 454, 4235
Di Criscienzo M. et al., 2013, MNRAS, 433, 313
Doherty C. L., Gil-Pons P., Lau H. H. B., Lattanzio J. C., Siess L., 2014, MNRAS, 437, 195
Ferrarotti A. D., Gail H. P., 2006, A&A, 553, 576
Fishlock C. K., Karakas A. I., Lugaro M., Yong D., 2014, ApJ, 797, 44
Frost C. A., Cannon R. C., Lattanzio J. C., Wood P. R., Forestini M., 1998, A&A, 332, L17
García-Hernández D. A., García-Lario P., Plez B., D'Antona F., Manchado A., Trigo-Rodríguez J. M., 2006, Science, 314, 1751
García-Hernández D. A., García-Lario P., Plez B., Manchado A., D'Antona F., Lub J., Habing H., 2007, A&A, 462, 711
García-Hernández D. A. et al., 2009, ApJ, 705, L31
García-Hernández D. A., Ventura P., Delgado-Inglada G., Dell'Agli F., Di Criscienzo M., Yague A., 2016, MNRAS, 458, L11
Gilroy K. K., 1989, ApJ, 347, 835
Gilroy K. K., Brown J. A., 1991, ApJ, 371, 578
Girardi L., Marigo P., 2007, A&A, 462, 237
Grevesse N., Sauval A. J, 1998, Space Sci. Rev., 85, 161
Groenewegen M. A. T., de Jong T., 1993, A&A, 267, 410
Groenewegen M. A. T. et al., 2007, MNRAS, 376, 313
Harris J., Zaritsky D., 2004, AJ, 127, 1531
Harris J., Zaritsky D., 2009, ApJ, 138, 1243
Henry R. B. C., Speck A., Karakas A. I., Ferland G. J., Maguire M., 2012, ApJ, 749, 61
Herwig F., 2005, ARA&A, 43, 435
Herwig F., Freytag B., Fuchs T., Hansen J. P., Hueckstaedt R. M., Porter D. H., Timmes F. X., Woodward P. R., 2007, in Kerschbaum F., Charbonnel C., Wing R. F., eds, ASP Conf. Ser. Vol. 378, Why Galaxies Care About AGB Stars: Their Importance as Actors and Probes. Astron. Soc. Pac., San Francisco, p. 43
Izzard R. G., Tout C. A., Karakas A. I., Pols O. R., 2004, MNRAS, 350, 407
Jacoby G. H., 1980, ApJS, 42, 1
Kamath D., Karakas A. I., Wood P. R., 2012, ApJ, 746, 20
Karakas A. I., Lattanzio J. C., 2014, PASA, 31, e030
Karakas A. I., Lattanzio J. C., Pols O. R., 2002, PASA, 19, 515
Keller S. C., Wood P. R., 2006, ApJ, 642, 834
Leisy P., Dennefeld M., 1996, A&AS, 116, 95
Leisy P., Dennefeld M., 2006, A&A, 456, 451
Maraston C., Daddi E., Renzini A., Cimatti A., Dickinson M., Papovich C., Pasquali A., Pirzkal N., 2006, ApJ, 652, 85
Marigo P., Aringer B., 2009, A&A, 508, 1538
Marigo P., Girardi L., Bressan A., 1999, A&A, 344, 123
Marigo P., Bernard-Salas J., Pottasch S. R., Tielens A. G. G. M., Wesselius P. R., 2003, A&A, 409, 619
Marigo P., Bressan A., Girardi L., Aringer B., Gullieuszik M., Groenewegen M. A. T., 2011, in Kerschbaum F., Lebzelter T., Wing R. F., eds, ASP Conf. Ser. Vol. 445, Why Galaxies Care about AGB Stars II: Shining Examples and Common Inhabitants. Astron. Soc. Pac., San Francisco, p. 431
Meyssonnier N., Azzopardi M., 1993, A&AS, 102, 451
Morgan D. H., Good A. R., 1985, MNRAS, 213, 491
Nanni A., Bressan A., Marigo P., Girardi L., 2013a, MNRAS, 434, 488
Nanni A., Bressan A., Marigo P., Girardi L., 2013b, MNRAS, 434, 2390
Nanni A., Bressan A., Marigo P. Girardi L., 2014, MNRAS, 438, 2328
Porter R. L., Bauman R. P., Ferland G. J., MacAdam K. B., 2005, ApJ, 622, L73
Pottasch S. R., Bernard- Salas J., 2006, A&A, 457, 189
Renzini A., Voli M., 1981, A&A, 94, 175
Riebel D., Meixner M., Fraser O., Srinivasan S., Cook K., Vijh U., 2010, ApJ, 723, 1195
Riebel D., Srinivasan S., Sargent B., Meixner M., 2012, AJ, 753, 71
Romano D., Karakas A. I., Tosi M., Matteucci F., 2010, A&A, 522, A32
Russell S. C., Dopita M. A., 1992, ApJ, 384, 508
Sanduleak N., Pesch P., 1981, PASP, 93, 431
Sanduleak N., MacConnell D. J., Philip A. G. D., 1978, PASP, 90, 621
Santini P. et al., 2014, A&A, 562, A30

Shaw R. A. et al., 2010, ApJ, 717, 562
Spite M., Barbuy B., Spite F., 1989, A&A, 222, 35
Srinivasan S. et al., 2009, AJ, 137, 4810
Srinivasan S., Sargent B. A., Meixner M., 2011, A&A, 532, A54
Stanghellini L., Blades J. C., Osmer S. J., Barlow M. J., Liu X.-W., 1999, ApJ, 510, 687
Stanghellini L., Shaw R. A., Balick B., Mutchler M., Blades J. C., Villaver E., 2003a, ApJ, 596, 997
Stanghellini L., Villaver E., Shaw R. A., Mutchler M., 2003b, ApJ, 598, 1000
Stanghellini L., Garcia-Lario P., García-Hernández D. A., Perea-Calderón J. V., Davies J. E., Manchado A., Villaver E., Shaw R. A., 2007, ApJ, 671, 1669
Stanghellini L., Lee T.-H., Shaw R. A., Balick B., Villaver E., 2009, ApJ, 702, 733
Stasińska G., Richer M. G., McCall M. L., 1998, A&A, 336, 667
Valiante R., Schneider R., Salvadori S., Bianchi S., 2011, MNRAS, 416, 1916
Ventura P., D'Antona F., 2005, A&A, 431, 279
Ventura P., D'Antona F., 2009, MNRAS, 499, 835
Ventura P., Zeppieri A., Mazzitelli I., D'Antona F., 1998, A&A, 334, 953
Ventura P., D'Antona F., Mazzitelli I., 2000, A&A, 363, 605
Ventura P., D'Antona F., Mazzitelli I., Gratton R., 2001, ApJ, 550, L65
Ventura P. et al., 2012a, MNRAS, 420, 1442
Ventura P. et al., 2012b, MNRAS, 424, 2345
Ventura P., Di Criscienzo M., Carini R., D'Antona F., 2013, MNRAS, 431, 3642
Ventura P., Di Criscienzo M. D., D'Antona F., Vesperini E., Tailo M., Dell'Agli F., D'Ercole A., 2014a, MNRAS, 437, 3274
Ventura P., Dell'Agli F., Di Criscienzo M., Schneider R., Rossi C., La Franca F., Gallerani S., Valiante R., 2014b, MNRAS, 439, 977
Ventura P., Karakas A. I., Dell'Agli F., Boyer M. L., García-Hernández D. A., Di Criscienzo M., Schneider R., 2015a, MNRAS, 450, 3181
Ventura P., Stanghellini L., Dell'Agli F., Garcia-Hernandez D. A., Di Criscienzo M., 2015b, MNRAS, 542, 3679 (Paper I)
Ventura P., Karakas A. I., Dell'Agli F., García-Hernández D. A., Boyer M. L., Di Criscienzo M., 2016, MNRAS, 457, 1456
Wachter A., Schröder K. P., Winters J. M., Arndt T. U., Sedlmayr E., 2002, A&A, 384, 452
Wachter A., Winters J. M., Schröder K. P., Sedlmayr E., 2008, A&A, 486, 497
Weiss A., Ferguson J. W., 2009, A&A, 508, 1343
Westerlund B. E., 1997, The Magellanic Clouds, Cambridge Univ. Press, Cambridge

This paper has been typeset from a TEX/LATEX file prepared by the author.